RSC Advances

PAPER

View Article Online
View Journal | View Issue

Cite this: *RSC Adv.*, 2025, **15**, 31597

High molecular weight polyethylene *via* the spatial proximity of benzosuberyl in iminopyridine nickel catalysts

Areej Khalid,[abc] Qaiser Mahmood,[*b] Ayesha Razzaq,[abc] Yanping Ma,[*a] Geng Ren,[a] Yizhou Wang,[ac] Tongling Liang[a] and Wen-Hua Sun[*abc]

Iminopyridine nickel catalysts are typically prone to facile chain transfer reactions, resulting in low molecular weight polyethylenes. In this study, a spatial proximity strategy was employed in 5-dibenzosuberyl-modified iminopyridine nickel catalysts to enhance ethylene polymerization. Using a template reaction between acetylpyridine and 5-dibenzosuberyl-functionalized aniline, a series of 2-(1-(2,6-bis(5-dibenzosuberyl)-4-(alkyl)phenylimino)ethyl)pyridine ligands were synthesized and subsequently reacted with (1,2-dimethoxyethane)$NiBr_2$ to afford the corresponding nickel complexes. Single-crystal X-ray diffraction revealed a sandwich-like arrangement in the resulting nickel complexes, with short centroid-to-plane distances (average: 3.194 Å for **Ni1^{Me}** and 3.268 Å for **Ni2^{iPr}**), suggesting close spatial proximity between the benzosuberyl phenyl caps and the chelate plane. Compared to DEAC, activation with MAO resulted in a higher activity (up to 2.2 × 10^6 g mol^{-1} h^{-1}), significantly increased molecular weights (56–182 kg mol^{-1}), and a narrower dispersity (PDI = 1.5–1.8). Notably, the polymer molecular weights were 10 to 100 times greater than those of most previously reported iminopyridine nickel catalysts lacking benzosuberyl steric substituents, indicating the strong and advantageous impact of the spatial proximity of benzosuberyl toward the chelate plane on polymerization. Moreover, in the case of substituent variations in the catalyst, dibenzosuberyl substituents at all the *ortho*- and *para*-positions of aniline demonstrated a positive effect on both the monomer insertion rate and chain propagation, leading to high catalytic activity and polymer molecular weights. The resulting polyethylene predominantly contained methyl branches, with an overall branching density of 53 to 99/1000C, as confirmed by high-temperature NMR measurements.

Received 26th July 2025
Accepted 18th August 2025

DOI: 10.1039/d5ra05407a

rsc.li/rsc-advances

Introduction

In coordination–insertion ethylene polymerization, the discovery of α-diimine Ni(II)/Pd(II) catalysts over two decades ago introduced strong candidates for producing highly branched polyethylene with high molecular weight and narrow dispersity.[1,2] The unprecedented chain-walking behavior of these catalysts eliminates the need for expensive higher-order α-olefins to induce branching, and thus, they are widely embraced in both industry and academia.[3,4] Molecular weight and branching are two important parameters of polyethylene, which are critical in determining its application across different sectors. For instance, highly branched, low-molecular-weight waxes are in high demand for use in lubricants, additives, co-monomers, coatings, and functional polymers.[5] In contrast, high-molecular-weight polyethylene with controlled branching is widely sought after in applications ranging from consumer electronics to packaging, automotive components, and photovoltaic encapsulants, where it serves as a thermoplastic elastomer that enhances product performance, design flexibility, and sustainability.[4,6,7]

Variations in nickel catalyst ligand structures significantly impact ethylene polymerization.[8] Diimine, iminopyridine, phenoxy-imine, ketone-imine, phosphine oxide, sulfonate, and phenoxide are ligand families still under active investigation for elucidation of their influence on the distinctive catalytic behavior of nickel catalysts, such as chain walking, chain transfer, and termination under various reaction conditions.[9] Among them, α-diimine- and iminopyridine-based catalysts are well established as robust chain-walking systems, producing highly branched polyethylene. However, iminopyridine nickel catalysts tend toward facile chain termination, generating typically low molecular weight polyethylene waxes or sticky

[a]*Key Laboratory of Engineering Plastics, Beijing National Laboratory for Molecular Science, Institute of Chemistry, Chinese Academy of Sciences, Beijing 100190, China. E-mail: myanping@iccas.ac.cn; whsun@iccas.ac.cn*

[b]*Chemistry and Chemical Engineering Guangdong Laboratory, Shantou 515031, China. E-mail: qaiser@ccelab.com.cn*

[c]*CAS Research/Education Center for Excellence in Molecular Sciences and International School, University of Chinese Academy of Sciences, Beijing 100049, China*

materials, largely due to the insufficient steric protection from their single *N*-aryl substituents.[2,9,10] The limited shielding of active species allows rapid chain transfer and catalyst deactivation, resulting in lower molecular weights. For example, nickel complex **A** (Fig. 1), reported by Laine and coworkers in 1999, exhibited a high catalytic activity (up to 6.8×10^6 g mol^{-1} h^{-1}) but produced polyethylene with low to moderate molecular weights (2.7–45.0 kg mol^{-1}).[11] Within the last two decades, modification of the iminopyridine framework, targeting steric and electronic substituents at the imine carbon(ı), pyridine ring (ii), and N-bound phenyl ring (iii), has been extensively explored.[10,12] A collection of representative modifications of the catalyst structure are given in Fig. 1(**B–G**).[13–18] (i) The incorporation of bulky substituents on the pyridine ring, particularly at position 6 of pyridine, in general, gives volatile oligomers or very low molecular weight polyethylene ($M_w \leq 1$ kg mol^{-1}), with activity and selectivity highly sensitive to steric and electronic perturbations (**E**, Fig. 1).[16] (ii) Similar trends were observed for modifications at the imine carbon, for example, carbocyclic fused iminopyridine-nickel catalysts showed significant improvements in activity and control over microstructure and chain-end groups (vinylene/vinyl up to 93.6%); however, they still produced low to moderate molecular weights (1.4–9.2 kg mol^{-1}) (**F**, Fig. 1).[17] (iii) Steric substituent variations on the *ortho* position of the N-bound phenyl ring show the most important role in determining activity, thermal stability, molecular weight, and dispersity (**B**-**D** and **G**, Fig. 1).[13–15,18] Except for the half-"sandwich" pyridine-imine nickel complex (**G**, Fig. 1),[18] all the others produced only low to moderate molecular weight polyethylene (0.9–22.1 kg mol^{-1}).[13–15] In contrast, complex **G** is the sole example that gave exceptionally high molecular weights, ranging from 10 to 1425 kg mol^{-1}.[18a] These findings underscore that steric bulk from *N*-aryl substituents, even when combined with imine-carbon modifications, cannot adequately regulate chain transfer, thereby constraining the synthesis of high molecular weight polyethylene essential for advanced applications.

Apart from steric and electronic tuning, recently, weak non-covalent interactions have gained prominence to tune the performance of catalysts in olefin polymerization.[19,20] In particular, intra-ligand π–π interactions curtail the rotation of the N-bound phenyl group, creating a rigid steric environment over the metal center. This steric hindrance helps to suppress chain transfer reactions and improve the molecular weight and other catalytic parameters. For example, π–π interactions in pyrazolylimine catalysts have shown higher thermal stability and yielded polyethylene with molecular weights up to 40 times greater than their counterparts lacking these interactions.[21,22] However, although non-covalent interactions are widely exploited in transition metal catalysts, their application in iminopyridine precatalysts for ethylene polymerization remains limited.[19] Very recently, during the preparation of this manuscript, a series of dibenzosuberyl-based iminopyridine-nickel catalysts was reported, with some structures partially overlapping with those presented in the current work.[18b] These catalysts exhibited high activity (in the range of 10^6 g mol^{-1} h^{-1}) for ethylene polymerization, affording polyethylenes with molecular weights ranging from 53.8 to 156.9 kg mol^{-1}. Motivated by the potential effect of the close spatial arrangement of steric groups, we have prepared a series of dibenzosuberyl-modified iminopyridine nickel catalysts for ethylene polymerization (**H**, Fig. 1). The distances between the centroids of the phenyl caps and the chelate plane indicate the spatial proximity of benzosuberyl toward the chelate plane, which may induce weak intramolecular interactions. As a result, these nickel catalysts exhibit high catalytic performances, particularly

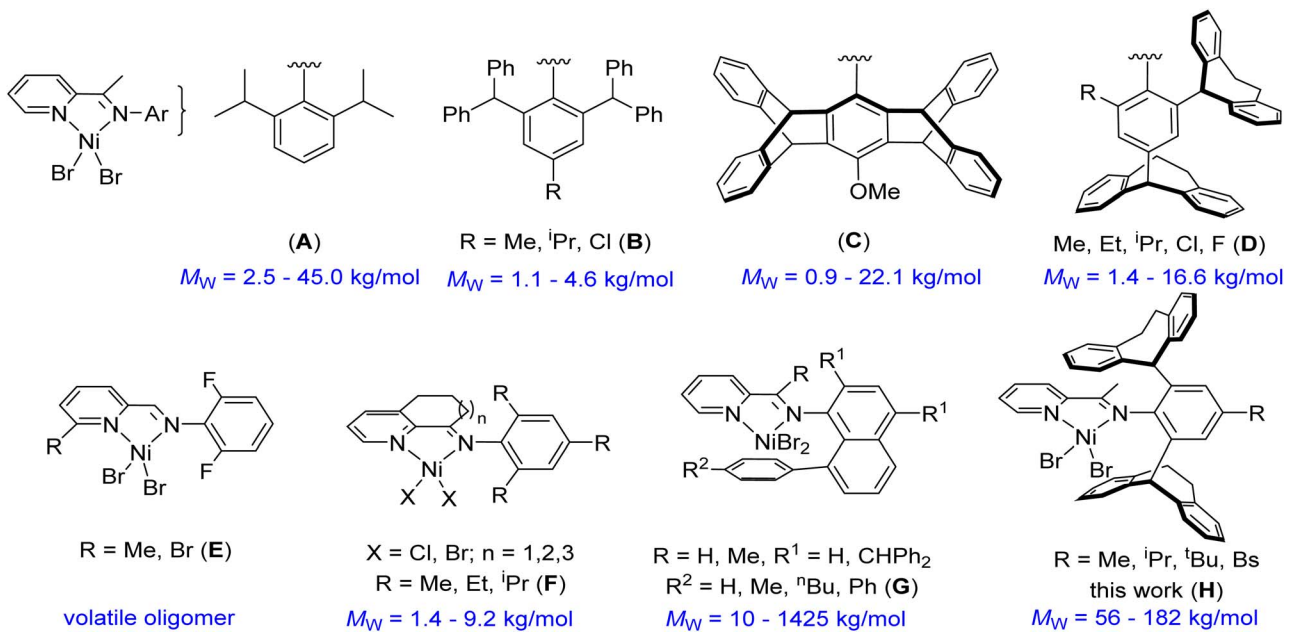

Fig. 1 Representative iminopyridine-nickel catalysts reported for ethylene polymerization ((A)–(G)), including those in this work (H), with the corresponding molecular weights of the resulting polyethylenes.

producing polyethylene with molecular weights significantly higher than previously reported iminopyridine-nickel systems lacking benzosuberyl steric substituents.

Results and discussion

Synthesis and characterization of ligands and their nickel complexes

The synthesis route for the iminopyridine ligands and their corresponding nickel complexes is shown in Scheme 1.[12f] The anilines used in ligand synthesis are not commercially available and were prepared *via* a Friedel–Crafts alkylation strategy.[22a,b] The ligands were obtained as yellow solids by the reaction of anilines with an equimolar amount of acetylpyridine. FT-IR, ^{1}H NMR, and ^{13}C NMR spectra verified the formation of the ligands, while elemental analysis confirmed their structural stability and purity. Treatment of the ligands with (1,2-dimethoxyethane)$NiBr_2$ at room temperature afforded a series of 2-(1-(2,6-bis(5-dibenzosuberyl)-4-(R)phenylimino)ethyl)pyridine nickel bromide complexes [R = Me for **Ni1^{Me}**, ^{i}Pr for **Ni2^{iPr}**, ^{t}Bu for **Ni3^{tBu}**, 5-dibenzosuberyl for **Ni4^{Bs}**] in good yields (76–89%). The resulting complexes were collected as dark-yellow to brown powders, which were stable to air and moisture. FT-IR spectra confirmed the ligand coordination to the nickel center, as evidenced by the shift in the imine stretching frequencies (ν(C=N)) from 1639–1647 cm^{-1} in the ligands to 1591–1622 cm^{-1} in the complexes.[12a,c,d] This shift to lower wavenumbers indicates the effective coordination of the ligand with the nickel center. Elemental analysis of carbon, hydrogen, and nitrogen further supported the proposed structures and purity of the complexes. Additionally, single-crystal X-ray diffraction analysis of **Ni1^{Me}** and **Ni2^{iPr}** verified their solid-state molecular structures.

Single crystals of **Ni1^{Me}** and **Ni2^{iPr}** suitable for X-ray diffraction analysis were independently grown from diethyl ether/*n*-hexane mixed solutions. The ORTEP representations of their molecular structures are shown in Fig. 2 and 3, respectively. Selected bond lengths and angles are given in the Table S1. Both structures exhibit a four-coordinate nickel center bonded to two nitrogen atoms from the bidentate iminopyridine ligand and two bromide ligands, forming a distorted tetrahedral geometry. The Ni–N and Ni–Br bond lengths fall within the expected range for this type of Ni(II) complex.[23] In **Ni1^{Me}**, the Ni1–N1 (pyridine) bond length is 1.997(3) Å, which is slightly shorter than the Ni1–N2 (imine) bond length of 2.012(3) Å (Table S1). A similar trend is observed in **Ni2^{iPr}**, likely due to the stronger coordination ability of the pyridine nitrogen compared to the imine nitrogen. The bond angles deviate from the ideal tetrahedral value (109.5°), likely due to steric hindrance from the bulky dibenzosuberyl substituents.[23] The phenyl ring attached to the imine nitrogen is found to tilt almost orthogonally to the chelate plane, which positioned the phenyl rings of the dibenzosuberyl groups directly above the imine bond and ligand backbone. As a result, the ligand backbone appears to be sandwiched between the phenyl rings of both dibenzosuberyl groups. The distances between the centroids of these phenyl caps and the chelate plane are calculated to be 3.202 Å and 3.185 Å for **Ni1^{Me}** and 3.274 Å and 3.262 Å for **Ni2^{iPr}**, respectively, which are lower than the sum of the van der Waals radii of C and C (3.4 Å).[19–22] These short distances suggest significant spatial proximity, which may induce weak intramolecular interactions. This sandwich-like arrangement and spatial

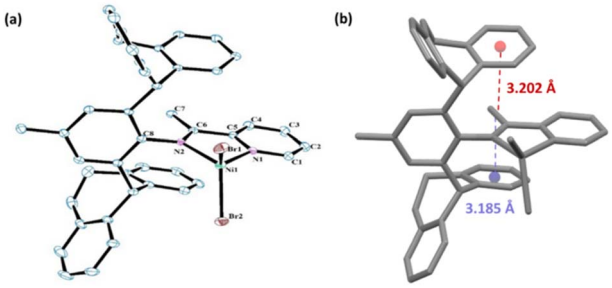

Fig. 2 (a) ORTEP view of the molecular structure of **Ni1^{Me}** and (b) front view with the calculated distance between the centers of the phenyl cap and plane of chelate; thermal ellipsoids are set at a 30% probability level, and hydrogen atoms are omitted for clear diagrams.

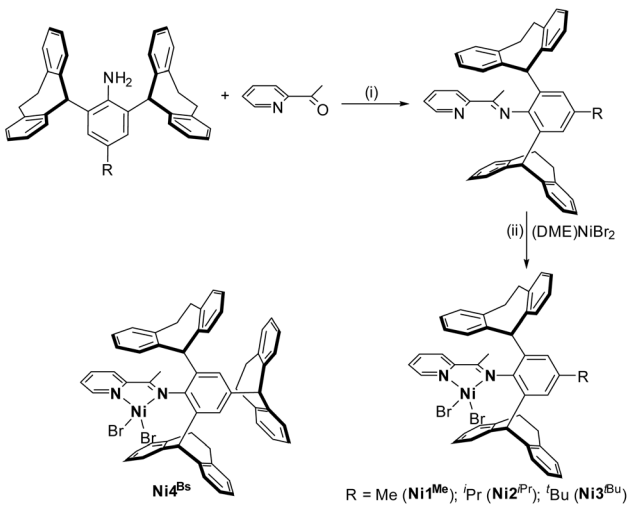

Scheme 1 Synthesis route of ligands and nickel complexes bearing a 5-dibenzosuberyl group. Conditions: (i) *p*-TsOH (cat.), toluene, reflux, 12 h; (ii) dichloromethane/ethanol, room temperature, inert atmosphere, overnight stirring.

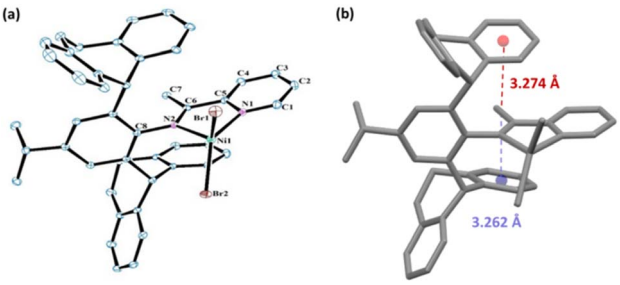

Fig. 3 (a) ORTEP view of the molecular structure of **Ni1^{iPr}** and (b) front view with the calculated distance between the centers of the phenyl cap and plane of chelate; thermal ellipsoids are set at a 30% probability level, and hydrogen atoms are omitted for clear diagrams.

proximity between the phenyl caps and the chelate plane in the catalyst structure are particularly important, which can strongly affect the accessibility of the nickel center and its catalytic behavior in polymerization reactions.

Ethylene polymerization

All the synthesized nickel complexes were evaluated as pre-catalysts with two optimal alkyl aluminum cocatalysts for ethylene polymerization.[24] In addition, the effects of cocatalyst concentration, reaction temperature, polymerization time, and ethylene pressure were systematically studied. These investigations were carried out in parallel using the two most effective cocatalysts. The units for polymerization activity and weight-average molecular weight were g mol^{-1} h^{-1} and g mol^{-1}, respectively; however, these units are not repeated throughout the text.

Selection of optimal cocatalysts

Activation of the nickel catalyst is an important aspect of ethylene polymerization, given that it strongly affects the catalysis, particularly the catalytic activity, molecular weight, and the melting point of the resulting polyethylene. Four alkyl aluminium cocatalysts were evaluated with the test precatalyst **Ni1^{Me}** under identical conditions including chloro-free methylaluminoxane (MAO) and modified methylaluminoxane (MMAO), and chloro-containing diethylaluminum chloride (DEAC) and ethylaluminum sesquichloride (EASC). The structure of these cocatalysts are given in Fig. S21. Table 1 presents the ethylene polymerization results using different cocatalysts. All cocatalysts showed high efficiency to activate **Ni1^{Me}** and showed notable variations in the activity and polymer properties. Among the chloro-free cocatalysts, MAO exhibited significantly higher activity but produced polyethylene with comparatively lower molecular weights (entries 1 and 2, Table 1). Possibly, MAO being smaller in size than MMAO can easily get access to the metal center, and therefore shows faster activation, as suggested by its high activity; however, easy access to the metal center also promotes chain transfer reactions. On the other hand, MMAO show better control over the chain transfer reaction and thus yields higher molecular weight polyethylene.[25] Among the chloro-containing cocatalysts, DEAC showed higher activity and produced polyethylene with relatively higher molecular weights (entries 3 and 4, Table 1). This difference likely arises from the varying number of chlorine groups in these two cocatalysts. Overall, the activity followed the trend of MAO > DEAC > MMAO ≈ EASC. These variations are strongly associated with the distinct physicochemical characteristics of each cocatalyst, such as their capacity for alkylation, degree of Lewis acidity, interaction strength with the growing polymer chain, and the steric and electronic attributes of the resulting organoaluminate counterions.[26,27] Based on the activity trend and the distinct influence of cocatalyst type on the polymerization behavior, MAO and DEAC were selected for further parallel investigations in ethylene polymerization.

Table 1 Screening of cocatalyst with **Ni1^{Me}** for ethylene polymerization[a]

Entry	Cocat.	Al/Ni	PE (g)	Act.[b] (10^6)	M_w[c] (10^4)	PDI[c]	T_m[d] (°C)
1	MAO	1500	1.5	1.5	7.0	1.7	54.6
2	MMAO	1500	0.6	0.6	10.5	1.8	56.4
3	EASC	400	0.6	0.6	8.0	2.1	57.7
4	DEAC	400	0.9	0.9	17.1	2.6	64.4

[a] Conditions: **Ni1^{Me}** (2.0 μmol); toluene (100 mL); C_2H_4 (1 MPa); 30 min; 30 °C. [b] Activity unit: g mol^{-1} h^{-1}. [c] M_w (unit: g mol^{-1}) determined by GPC. [d] T_m determined by DSC.

Optimization of reaction conditions for Ni1^{Me}/DEAC

Four reaction parameters, namely, Al/Ni ratio, temperature, time and ethylene pressure, were investigated individually with **Ni1^{Me}** under identical conditions; the best conditions found were then used for all the precatalysts as standard conditions to find the best precatalyst structure for ethylene polymerization.

Entries 1–6 in Table 2 summarize the polymerization results using different Al/Ni ratios under identical conditions, and the data are graphically presented in Fig. 4a. Cocatalyst optimization aims to identify the amount that gives the highest catalytic activity, given that insufficient cocatalyst may not fully activate the catalyst, while excessive amounts can lead to side reactions, the formation of multiple active species, or deactivation of the metal center.[28] The results showed that the activity gradually increased with an increase in cocatalyst from 400 to 800 equiv. relative to **Ni1^{Me}**. The maximum activity of 1.4×10^6 was observed at an Al/Ni ratio of 800 (entry 4, Table 2), followed by a gradual decline to 1.1×10^6 at Al/Ni = 1000 (entry 6, Table 2). Correspondingly, polymer molecular weights decreased with increase of cocatalyst concentration. The highest M_w of 17.1×10^4 was observed at Al/Ni = 400, while the lowest, 5.8×10^4, was found at the highest ratio tested. Typically, alkylaluminium cocatalysts not only activate the metal center but also participate in side reactions, particularly chain transfer processes, which shift the growing polymer chain from the nickel to aluminum center.[29] These reactions become more prominent at higher cocatalyst concentrations, resulting in lower molecular weights. Despite the variations in cocatalyst loading, the molecular weight distributions remain narrow and unimodal, indicating single-site polymerization behavior, with dispersity ranging from 1.6 to 2.8. This behavior is consistent with previous reports.[12]

The polymerization temperature is the most influential parameter, which greatly affects the activity, molecular weight, and microstructure of the resulting polyethylene. To investigate this, polymerization tests were performed at 30 °C, 40 °C, and 50 °C under identical conditions and the results are summarized in entries 4, 8 and 9 of Table 2 (Fig. 4b), respectively. Compared to 30 °C, polymerization at 40 °C showed approximately 20% increase in activity, accessing the highest activity of 1.7×10^6 (entry 8, Table 2), while a further increase to 50 °C resulted in a 40% decrease in activity (entry 9, Table 2). This decrease in activity may result from the decomposition of the active species and decreased ethylene solubility at elevated

Table 2 Screening of DEAC amount, temperature, time and ethylene pressure for ethylene polymerization using **Ni1^{Me}**/DEAC[a]

Entry	Al/Ni	T (°C)	t (min)	PE (g)	Act.[b] (10^6)	M_w[c] (10^4)	PDI[c]	T_m[d] (°C)
1	400	30	30	0.9	0.9	17.1	2.6	64.4
2	600	30	30	1.2	1.2	14.1	2.8	65.2
3	700	30	30	1.3	1.3	10.7	2.3	69.5
4	800	30	30	1.4	1.4	9.8	2.4	64.1
5	900	30	30	1.2	1.2	9.5	2.1	64.9
6	1000	30	30	1.1	1.1	5.8	1.6	67.1
7	800	40	30	1.7	1.7	6.9	2.1	56.8
8	800	50	30	1.0	1.0	6.3	2.1	55.9
9	800	40	5	0.3	1.9	6.2	2.1	55.6
10	800	40	15	0.9	1.8	6.3	1.9	56.1
11	800	40	45	1.9	1.3	10.0	3.1	56.6
12	800	40	60	2.4	1.2	11.9	3.7	57.8
13[e]	800	40	30	0.6	0.6	6.5	2.1	49.4
14[f]	800	40	30	1.0	1.0	7.2	2.0	49.9

[a] Conditions: **Ni1^{Me}** (2.0 μmol); toluene (100 mL); C_2H_4 (10 atm). [b] Activity unit: g mol^{-1} h^{-1}. [c] M_w (unit: g mol^{-1}) determined by GPC. [d] T_m determined by DSC. [e] 1 atm ethylene. [f] 5 atm ethylene.

temperatures.[30] Higher temperatures may also promote chain termination, as indicated by the gradual decline in molecular weight from 9.8 × 10^4 at 30 °C to 6.3 × 10^4 at 50 °C, representing a decrease of approximately 35%.[31] As shown in Fig. S17, the GPC traces of the resulting polyethylene are unimodal with PDI in the range of 2.1 to 2.4, indicating the single-site behavior of the catalyst.

Time-dependent ethylene polymerization was subsequently investigated under identical conditions (entries 4 and 9–12, Table 2). The results revealed clear trends, where both the polymer yield and molecular weight showed an approximately linear dependence on reaction time, with coefficients of determination (R^2) of 0.988 and 0.921, respectively (Fig. 4c). The polymer yield increased from 0.3 g for 5 min to 2.4 g for 60 min, indicating that the metal center remains active throughout the reaction. Meanwhile, the consistent increase in polymer molecular weights from 6.2 × 10^4 to 11.9 × 10^4 reflects continuous chain propagation over time. However, despite these trends, the catalytic activity showed a gradual decline from 1.9 × 10^6 to 1.2 × 10^6 over the course of the reaction

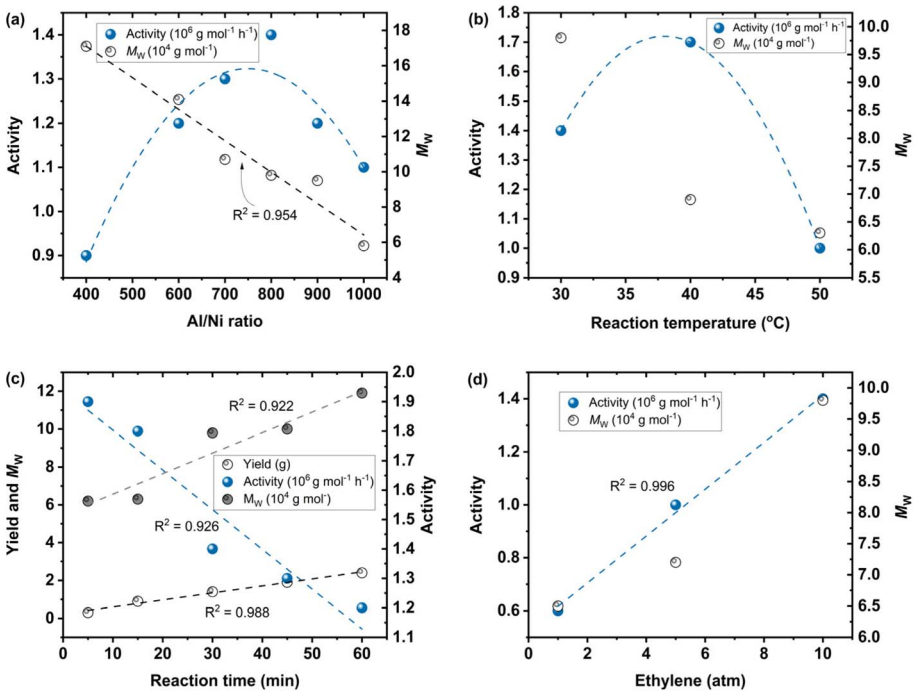

Fig. 4 Relationship between catalytic activity and molecular weight with respect to (a) Al/Ni ratio, (b) reaction temperature, (c) polymerization time, and (d) ethylene pressure.

(Fig. 4c). This decrease may be attributed to the partial deactivation of the active species or increased polymer mass in the reaction medium, which ultimately reduces the catalyst efficiency.[32] Similar kinetic profiles have been reported for α-diimine Ni(II) systems, where although the high initial activity significantly drops, the polymer molecular weight continually grows with prolongation of the reaction duration.[22] The polymer dispersity values remained unimodal and consistent during the initial 5 to 30 min of reaction (M_w/M_n = 1.9–2.4). However, polyethylene obtained after 45 and 60 min exhibited unimodal distributions with a shoulder at higher molecular weight and broader dispersity (3.1–3.7), suggesting enhanced chain transfer events or minor site heterogeneity as the reaction progressed. Overall, these findings align well with the previously reported kinetic behaviors of α-diimine-based catalysts.[22a]

The influence of ethylene pressure on polymerization performance was evaluated at 1, 5, and 10 atm under identical conditions (entries 4, 13 and 14, Table 2). As shown in Table 2, the catalytic activity increased significantly to a maximum of 1.4 × 10^6 at 10 atm compared to 1.0 × 10^6 and 0.6 × 10^6 at 1 and 5 atm, respectively (Fig. 4d). This enhancement is attributed to the higher monomer concentration available at elevated pressures, which facilitates faster chain propagation. The molecular weight followed a similar trend, which increased from 6.5 × 10^4 at 1 atm to 9.8 × 10^4 at 10 atm. The higher pressure not only promotes polymer growth but also leads to increased crystallinity, as evidenced by the increase in melting temperature from 49 °C at lower pressures to 64 °C at 10 atm.[33] The polymer dispersity remained relatively constant (2.0–2.4), indicating that pressure variations did not significantly affect the polymer chain distribution.

Evaluation of ligand design using DEAC cocatalyst

To evaluate the influence of *para*-substituent on the N-bound aryl groups on the nickel complexes for ethylene polymerization, all the title nickel bromide complexes were investigated under the conditions optimized for **Ni1^{Me}** [Al/Ni = 800, temperature = 40 °C, time 30 min, ethylene 1 atm]. The results are given in Table 1.

As shown in Fig. 5, the change in *para*-substituent of N-bound aryl group gave a clear relationship with activity and properties of obtained PE such as molecular weight, melting point and branching density (entries 1–3, Table 3), respectively.

Table 3 Screening of different precatalysts using DEAC as the cocatalyst under the optimal conditions for ethylene polymerization[a]

Entry	Precat.	PE (g)	Act.[b] (10^6)	M_w[c] (10^4)	PDI[c]	T_m[d] (°C)	BD[e]
1	**Ni1^{Me}**	1.7	1.7	6.9	2.1	56.8	60
2	**Ni2^{iPr}**	1.2	1.2	7.5	2.1	63.6	66
3	**Ni3^{tBu}**	1.0	1.0	7.9	1.9	65.7	76
4	**Ni4^{Bs}**	2.0	2.0	8.2	2.0	64.1	99

[a] Conditions: precatalyst (2.0 μmol), toluene (100 mL), C_2H_4 (10 atm), Al/Ni (800), 30 min, 40 °C. [b] Activity unit. g mol^{-1} h^{-1}. [c] M_w (unit: g mol^{-1}) determined by GPC. [d] T_m determined by DSC. [e] BD = branching density/1000C determined from ^{1}H spectra [(2 × I_{Me}/3 × I_{total}) × 1000].

Among the first three complexes, **Ni1^{Me}** bearing an Me group (R = Me) displayed the highest activity of 1.7 × 10^6 and produced the lowest molecular weight polyethylene (M_w = 6.9 × 10^4) with controlled dispersity of 2.1 (entry 1, Table 3). In contrast, the **Ni3^{tBu}** (R = ^{t}Bu) complex bearing a sterically larger group was the least active but produced polyethylene with the highest molecular weight and comparatively narrow dispersity. The **Ni2^{iPr}** complex bearing an *i*Pr group, being intermediate in size, showed catalytic activity and polymer molecular weights in between that of **Ni1^{Me}** and **Ni3^{tBu}**. This correlation clearly indicates that increasing the steric hindrance at the distal position leads to reduced catalytic activity, while the opposite trend is observed for the molecular weight of the resulting polyethylene (Fig. 5a and b).[34] The Me group, being the smallest, interacts only weakly with the *ortho*-dibenzosuberyl moiety, resulting in a more open coordination environment for the monomer in **Ni1^{Me}**. In contrast, the ^{t}Bu group, being larger in size, in **Ni3^{tBu}** likely forces the *ortho*-dibenzosuberyl substituent toward the axial positions, and thus increases the steric congestion around the metal center. Consequently, **Ni1^{Me}** generates a sterically more open structure, while **Ni3^{tBu}** forms a more crowded environment and **Ni2^{iPr}** with an *i*Pr group creates a steric profile in between that of **Ni1^{Me}** and **Ni3^{tBu}**. Typically, a more open coordination sphere facilitates easier monomer coordination and insertion but at the same also gives high opportunities for chain transfer reaction, leading to lower molecular weight polymers. Conversely, a more hindered environment effectively suppresses chain transfer events, favoring the formation of higher molecular weight polyethylene, though

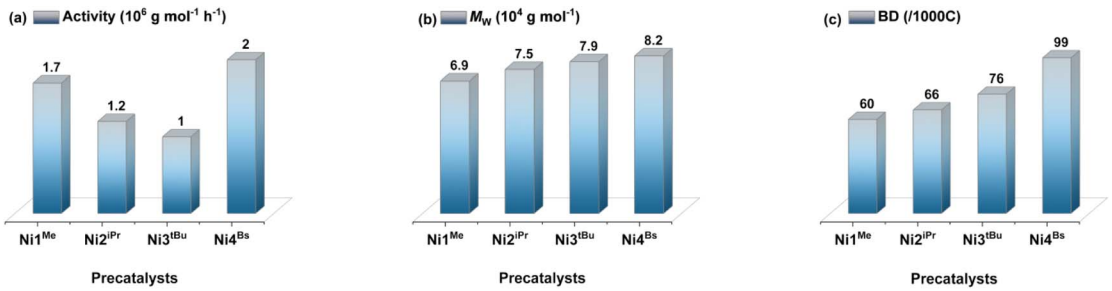

Fig. 5 Relationship of (a) activity, (b) molecular weight, and (c) branching density with the structure of the precatalysts using DEAC as the cocatalyst.

at the expense of reduced monomer access to the active site.[35] Moreover, compared to the three above-discussed nickel complexes, **Ni4^{Bs}** bearing a significantly bulkier *para*-substituent than Me, ^{i}Pr, or ^{t}Bu, exhibited catalytic activity of 2.0×10^6, which is approximately 18%, 67%, and 100% higher than that of **Ni1^{Me}**, **Ni2^{iPr}**, and **Ni3^{tBu}**, respectively (Fig. 5a). It is proposed that the much larger *para*-substituted dibenzosuberyl moiety in **Ni4^{Bs}** interacts strongly with the *ortho*-substituted dibenzosuberyl group, inducing intermolecular repulsion.[36] This repulsion may force the *ortho*-substituent to tilt into a position that gives relatively lower axial steric hindrance compared to the other three complexes. As a result, **Ni4^{Bs}** likely generates a more open coordination environment, facilitating rapid monomer coordination-insertion and chain growth processes. Although these open structures are typically prone to chain transfer reactions, often leading to lower molecular weight polymers, the exceptionally high rate of monomer insertion in this case appears to offset chain transfer, yielding polyethylene of molecular weight comparable to that produced by the other three catalysts. Beyond simple steric effects, the close spatial arrangement of the benzosuberyl groups may also influence the orientation and approach of ethylene monomers toward the nickel center, promoting more efficient insertion into the growing polymer chain. This controlled orientation stabilizes the chain-end and reduces undesired chain transfer events, allowing the catalyst to sustain rapid propagation. Thus, the molecular weights of polyethylene produced by all the nickel catalysts are approximately 10-times higher than that reported for previously studied iminopyridine nickel systems lacking benzosuberyl steric substituents.[13–17] This enhancement is most likely due to the spatial proximity of benzosuberyl toward the chelate plane, which may induce weak intramolecular interactions that suppress the rotation of the N-bound aryl group, thereby positioning the bulky dibenzosuberyl group more effectively over the axial sites and creating a more rigid catalyst structure. The resulting enhanced shielding of the metal center protects the growing polymer chain from chain transfer reactions, leading to the formation of polyethylene with significantly higher molecular weights.

Mechanistic investigations of the parent Brookhart catalyst for ethylene polymerization have shown that increased steric hindrance at the axial sites favors chain walking over chain propagation.[3] Numerous recent studies involving sterically varied substituents have further validated this conclusion.[2,7] Our current results based on branching density calculations from ^{1}H NMR spectroscopy also support this trend (Fig. 5c). For example, the **Ni1^{Me}** complex, being the least hindered, produced polyethylene with a branching density of 60/1000C. In contrast, **Ni2^{iPr}**, with greater steric bulk, yielded polyethylene with 66/1000C. Of significant note, **Ni3^{tBu}**, the most sterically hindered complex, resulted in significantly higher branching, with 76/1000C. In contrast, **Ni4^{Bs}**-based polyethylene exhibited a significantly higher branching density (99/1000C). This may be attributed to the steric repulsion between the *ortho*- and *para*-dibenzosuberyl groups, which could enforce a specific orientation of the *ortho*-substituent that promotes chain walking, thereby generating a higher number of branches. The

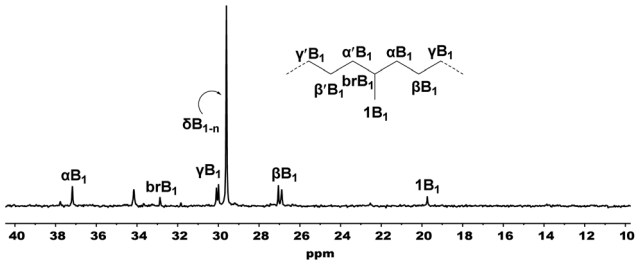

Fig. 6 ^{13}C NMR spectrum of polyethylene obtained at 30 °C using the Ni1^{Me}/DEAC catalyst system.

measured melting temperatures (T_m) ranged from 54.6 °C to 69.5 °C and were influenced by both the molecular weight and branching density. To clarify the branch content, a representative polyethylene sample synthesized using **Ni1^{Me}** at 30 °C with DEAC was analyzed *via* high-temperature ^{13}C NMR spectroscopy (Fig. 6).[37] This sample exhibited 60/1000C, consisting of methyl branches dominantly. These findings indicate that the resulting polyethylenes are primarily composed of short branches, with only a minor proportion of long branches.

Optimization of reaction conditions for Ni1^{Me}/MAO

For comparison purposes and to gain a deeper understanding of the effect of Cl-free alkylaluminium cocatalysts, ethylene polymerization was re-investigated using MAO. MAO is widely used in late transition metal catalysis due to its dual role as an alkylating agent and a stabilizing medium for cationic species, often enhancing both the catalytic activity and thermal stability compared to simple alkylaluminium compounds. **Ni1^{Me}** was again used as the test precatalyst to identify the optimal conditions, which were then applied to assess the influence of ligand structure. The results of cocatalyst concentration screening and reaction temperature variation are summarized in Table 4.

The effect of cocatalyst concentration on ethylene polymerization using **Ni1^{Me}** and MAO was systematically studied under identical conditions, and the results are summarized in entries 1–6 of Table 4. The highest activity of 2.1×10^6 was observed at

Table 4 Screening of MAO amount and reaction temperature for ethylene polymerization using Ni1^{Me}/MAO[a]

Entry	Al/Ni	T (°C)	PE (g)	Act.[b] (10^6)	M_w[c] (10^4)	PDI[c]	T_m[d] (°C)
1	1000	30	0.4	0.4	18.2	2.8	67.5
2	1500	30	1.5	1.5	13.2	1.9	70.2
3	1750	30	1.8	1.8	12.5	1.9	58.7
4	2000	30	2.1	2.1	12.3	1.5	61.9
5	2250	30	1.6	1.6	11.1	1.7	71.1
6	2500	30	1.1	1.1	10.7	1.8	62.3
7	2000	40	0.7	0.7	7.7	1.6	63.9
8	2000	50	0.5	0.5	5.6	1.9	58.6

[a] Conditions: **Ni1^{Me}** (2.0 μmol); toluene (100 mL); C_2H_4 (10 atm). [b] Activity unit: g mol^{-1} h^{-1}. [c] M_w (unit: g mol^{-1}) determined by GPC. [d] T_m determined by DSC.

an Al/Ni ratio of 2000 (entry 4, Table 4), while lower cocatalyst loadings resulted in significantly reduced activity (entries 1–3, Table 4). For example, at Al/Ni ratios of 1000–1750, the activity ranged from 0.4×10^6 to 1.8×10^6, which suggests insufficient alkylation or incomplete formation of the active species.[28] Conversely, increasing the MAO concentration beyond 2000 also led to a decline in activity. The activity decreased from 1.6×10^6 at 2250 to 1.1×10^6 at 2500, respectively. This reduction may be attributed to over-quenching of the active sites, resulting in a lower propagation efficiency. A similar trend was observed in the case of the DEAC cocatalyst (Table 2). In terms of molecular weight, a gradual decrease from 18.2×10^4 to 10.7×10^4 was observed with an increase in MAO concentration, likely because of the high chain transfer reactions at higher MAO loadings. The narrow dispersity (PDI = 1.5) at Al/Ni of 2000 further supports the conclusion that this ratio offers the best balance between catalytic activity and polymer quality. In the screening of optimal reaction temperature, the highest activity of 2.1×10^6 was observed at 30 °C (entry 4, Table 4). As the temperature increased, a decline in activity was recorded, *i.e.*, 0.7×10^6 at 40 °C and 0.5×10^6 at 50 °C (entries 7 and 8, Table 4), respectively. Similar to the trend observed with DEAC, this decrease in activity is likely due to the thermal decomposition of the active catalyst species and reduced solubility of ethylene at elevated temperatures.[30] The molecular weight of the resulting polyethylene also decreased with an increase in temperature from 12.3×10^4 at 30 °C to 5.6×10^4 at 50 °C. This trend suggests that higher temperatures promote chain transfer reactions, leading to shorter polymer chains.[31] The increase in molecular weight distribution from 1.5 to 1.9 further supports the presence of enhanced chain transfer at elevated temperatures. Despite this, the dispersity remained relatively narrow and unimodal across all conditions, indicating the operation of a single-site mechanism during polymerization.

Table 5 Screening of different precatalysts using MAO as the cocatalyst under the optimal conditions for ethylene polymerization[a]

Entry	Precat.	PE (g)	Act.[b] (10^6)	M_w[c] (10^4)	PDI[c]	T_m[d] (°C)	BD[e]
1	**Ni1^{Me}**	2.1	2.1	12.3	1.5	61.9	53
2	**Ni2^{iPr}**	1.3	1.3	12.6	1.6	68.3	63
3	**Ni3^{tBu}**	0.5	0.5	12.9	1.6	74.9	72
4	**Ni4^{Bs}**	2.2	2.2	13.5	1.8	68.1	96

[a] Conditions: precatalyst (2.0 μmol), toluene (100 mL), C_2H_4 (10 atm), Al/Ni (2000), 30 min, 30 °C. [b] Activity unit: g mol^{-1} h^{-1}. [c] M_w (unit: g mol^{-1}) determined by GPC. [d] T_m determined by DSC. [e] BD = branching density/1000C determined from ^{1}H spectra [$(2 \times I_{Me}/3 \times I_{total}) \times 1000$].

Evaluation of ligand design using MAO cocatalyst

The nature of the *para*-substituent on the *N*-aryl moiety had a pronounced impact on the catalytic behavior in ethylene polymerization (entries 1–4, Table 5) (Fig. 7). The observed trends in activity, molecular weight, melting point, and branching density closely resemble that obtained with the DEAC cocatalyst (Fig. 5 and 7). Among the catalytic performances in entries 1–3, **Ni3^{tBu}** (R = *t*Bu), bearing a sterically hindered *tert*-butyl group, was the least active (activity = 0.5×10^6) and produced polyethylene with a high branching density (BD = 72/1000C). In contrast, **Ni1^{Me}**, bearing the least hindered methyl group, exhibited the highest activity (2.1×10^6) and yielded polyethylene with the lowest branching density (BD = 53/1000C). **Ni2^{iPr}**, with an isopropyl substituent, showed an intermediate performance, with activity of 1.3×10^6 and branching density of 63/1000C. This trend suggests that the steric repulsion between the bulky ^{t}Bu group and the *ortho*-dibenzosuberyl groups in **Ni3^{tBu}** likely increases the axial hindrance. A more open coordination environment promotes faster monomer insertion relative to chain walking, while increased steric hindrance favors chain walking due to the comparatively lower rate of monomer insertion.[35] However, **Ni4^{Bs}**, which bears *para*-dibenzosuberyl groups in addition to *ortho*-dibenzosuberyl groups, deviates from this trend. It exhibits the highest activity (2.2×10^6, close to that of **Ni1^{Me}**) and produces polyethylene with the highest branching density (BD = 96/1000C) (entry 4, Table 5). This exceptional behavior may arise from the steric repulsion between the large *ortho*- and *para*-dibenzosuberyl groups, potentially reorienting the *ortho*-substituents and reducing the axial hindrance. This configuration could create a more accessible coordination environment that supports rapid monomer insertion while still enabling a high degree of chain walking. As a result, **Ni4^{Bs}** outperforms the other catalysts in both activity and branching without significantly compromising the molecular weight. The molecular weight of the resulting polyethylene was nearly similar,

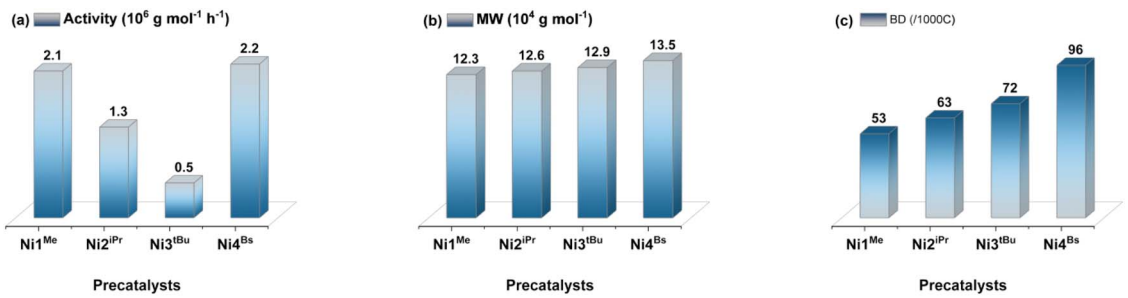

Fig. 7 Relationship of (a) activity, (b) molecular weight, and (c) branching density with the structure of the precatalysts using MAO as the cocatalyst.

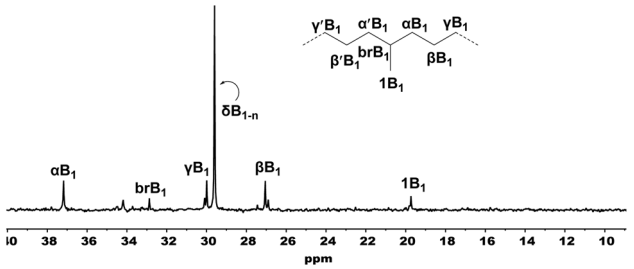

Fig. 8 ^{13}C NMR spectrum of polyethylene obtained at 30 °C using the **Ni1^{Me}**/MAO catalyst system.

ranging from 12.3 × 10^4–12.9 × 10^4 for the **Ni1^{Me}**, **Ni2^{iPr}** and **Ni3^{tBu}** complexes, while **Ni4^{Bs}** gave a slightly higher molecular weight of 13.5 × 10^4 with a controlled molecular weight dispersity (PDI = 1.5–1.8) and moderate polymer melting temperature in the range of 61.9–74.9 °C. These molecular weights are 10 to 100 times higher than those reported for previously studied iminopyridine nickel catalysts lacking benzosuberyl steric substituents.[11–17] This enhancement is likely due to the spatial proximity of benzosuberyl toward chelate plane, which may induce weak intramolecular interactions that rigidify the catalyst structure and restrict *N*-aryl rotation. The limited rotation of the N-bound phenyl group may better shield the active species, thereby promoting the formation of high molecular weight polyethylene.[19–22] High-temperature ^{13}C NMR of the resulting PE using **Ni1^{Me}**/MAO revealed that the resulting polyethylene had branches mainly composed of methyl branches similar to that of the **Ni1^{Me}**/DEAC-based polyethylene under similar conditions (Fig. 8). Thus, the **Ni1^{Me}**/DEAC-based PE displayed a slightly lower melting point (56.8 °C) and higher branching density than its MAO counterpart (T_m = 61.9 °C, BD = 53), further supporting the conclusion that the MAO system produces more crystalline and less branched polyethylene.

The comparison of the DEAC- and MAO-based studies on ethylene polymerization reveals similar trends in activity, molecular weight, and branching degree on changing the catalyst structure. However, polymerization with MAO showed in general slightly higher activity, significantly increased molecular weights, narrower dispersity, and slightly higher melting temperatures, while the branching density remained similar. For example, **Ni4^{Bs}** activated with DEAC exhibited an activity of 2.0 × 10^6, producing polyethylene with an M_w of 8.2 × 10^4, dispersity of 2.0, melt temperature of 64.1 °C, and branching density of 99/1000C. The same catalyst on activation with MAO showed a slightly higher activity of 2.2 × 10^6, a significantly higher M_w of 13.5 × 10^4, a narrower dispersity of 1.8, a slightly higher T_m of 68.1 °C, and a slightly lower BD of 96/1000C. These differences are primarily attributed to the nature of the cocatalyst and its interaction with the active metal center. DEAC, being smaller in size and a monomeric Lewis acid, facilitates efficient halide abstraction and rapid alkylation, generating highly reactive cationic species.[26,27] However, its strong interaction with the nickel center may also accelerate chain transfer and catalyst deactivation, especially at higher concentrations. In contrast, MAO, with its oligomeric structure and weaker coordination to the active site, provides a more flexible environment for generating and stabilizing the active species.[25] This results in longer catalyst lifetimes and, in some cases, increased branching in the resulting polymers.

Comparison with reported iminopyridine nickel catalysts

A comparison is made between the present work and previously reported iminopyridine nickel complexes for ethylene polymerization (Fig. 1, Table 6). The best catalytic activities under comparable conditions, along with the molecular weight (M_w or M_n) of the resulting polyethylene, are summarized in Table 6. Catalysts **A–E** exhibited activities in the range of 3.0–7.9 × 10^6, with a significant variation in polymer molecular weight (900–9350 g mol^{-1}, entries 1–5, Table 6). For example, catalyst **A** produced low-molecular-weight PE (M_w = 2500 g mol^{-1}) with activity of 6.8 × 10^6, whereas catalyst **D** displayed the highest activity in this group and afforded higher-molecular-weight polymer. In contrast, catalyst **E** produced only oligomeric material, indicating its insufficient chain-propagation efficiency. The **F**-series catalysts (**F**, n = 1, 2 or 3) highlight the influence of the fused carbocyclic ring size. Catalyst **F** (n = 1) delivered the highest activity among the tested systems (12.4 × 10^6), although the resulting polymer had a relatively modest molecular weight (3400 g mol^{-1}, entry 6). Increasing the ring size to seven carbons (n = 2) slightly reduced the activity but increased the molecular weight to 4535 g mol^{-1} (entry 7, Table 6). Further expansion to eight carbons (n = 3) caused a decline in both activity (3.44 × 10^6) and molecular weight (2700 g mol^{-1}, entry 8), suggesting that the carbocyclic ring size governs the balance between chain propagation and chain-transfer events. Catalyst **G** distinguished itself by producing high-molecular-weight polyethylene (83 000 g mol^{-1}) with activity of 4.3 × 10^6 (entry 9). Most notably, catalyst **H** (this work) afforded the highest molecular weight PE (135 000 g mol^{-1}) with activity of 2.2 × 10^6 (entry 10, Table 6). This result demonstrates

Table 6 Comparison of catalytic performance of iminopyridine nickel complexes in ethylene polymerization

Entry	Precat.	T (°C)	t (min)	Act. (10^6)	M_w or M_n	PDI
1[a]	**A**	40	15	6.8	2.5	1.6
2[b]	**B**	20	20	3.5	3.9	1.9
3[c]	**C**	30	30	4.7	0.9	2.1
4[d]	**D**	30	30	7.9	9.3	2.3
5[e]	**E**	35	15	3.0	[k]	[k]
6[f]	**F** (n = 1)	20	20	12.4	3.4	2.0
7[g]	**F** (n = 2)	20	30	7.8	4.5	1.9
8[h]	**F** (n = 3)	20	30	3.4	2.7	1.9
9[i]	**G**	20	30	4.3	83.0	1.7
10[j]	**H** (this work)	30	30	2.2	135.0	1.8

Conditions: activity: g mol^{-1} h^{-1}, M_w or M_n = 10^3 g mol^{-1}. [a] MAO (Al/Ni = 2000). [b] EASC (Al/Ni = 300). [c] DEAC (Al/Ni = 1000). [d] MAO (Al/Ni = 2500). [e] MAO (Al/Ni = 500). [f] DEAC (Al/Ni = 500). [g] MAO (Al/Ni = 2500). [h] DEAC (Al/Ni = 600). [i] DEAC (Al/Ni = 1000). [j] MAO (Al/Ni = 2000). [k] Oligomer.

that the current catalyst design promotes controlled chain propagation and suppresses chain transfer, enabling the formation of very long polymer chains at the expense of polymerization rate.

Conclusion

In summary, a series of 5-dibenzosuberyl-modified iminopyridine nickel catalysts was synthesized and evaluated for ethylene polymerization. Single-crystal X-ray diffraction confirmed the close spatial proximity of the benzosuberyl groups to the chelate plane, which significantly influenced the polymerization behavior. These structural features effectively suppressed the chain transfer events, resulting in significantly increased polymer molecular weights (up to 182 kg mol^{-1}) with narrow dispersity (PDI = 1.5–1.8), particularly when activated with MAO. A systematic evaluation of the cocatalysts showed that MAO outperformed DEAC, affording higher activity (up to 2.2×10^6 g mol^{-1} h^{-1}), higher molecular weights, and better control over dispersity. Additionally, ligand modification at the *para*-position modulated the catalytic behavior, where increased steric bulk reduced the activity but enhanced the molecular weight and branching density. Most importantly, the **Ni4^{Bs}** complex, bearing dibenzosuberyl substituents at both the *ortho* and *para* positions, demonstrated a combination of high activity, high molecular weight, and controlled dispersity, outperforming most previously reported iminopyridine systems. High-temperature NMR analysis confirmed predominantly methyl branches, correlating well with the observed melting points and crystallinity.

Experimental

Synthesis and characterization of ligands

L1^{Me}. Acetylpyridine (0.4 g), toluene (25 mL), aniline (1.62 g, 3.33 mmol), and *p*-toluenesulfonic acid (20%) were added to a 250 mL two-neck flask and heated at 140 °C. The reaction mixture was then refluxed for 60 min. After 12 h of heating and stirring, the reaction was stopped, and the mixture was allowed to cool to room temperature. A precipitate formed in the flask, which was collected by filtration and purified using *n*-hexane and ethyl acetate (v/v = 500 : 7) as the eluent on an alumina column. The desired product was obtained as a light-yellow powder (0.3 g, yield 15%). FT-IR (KBr, cm^{-1}): 3452 (w), 3056 (m), 3016 (m), 2927 (s), 2159 (w), 1970 (w), 1638 (ν(C=N), m), 1566 (ν(C=N), m), 1489 (m), 1444 (s), 1363 (s), 1303 (m), 1214 (m), 1134 (w), 1102 (s), 1045 (m), 994 (w), 946 (w), 875 (m), 1048 (w), 817 (s), 873 (w), 735 (w). ^{1}H NMR (400 MHz, $CDCl_3$, TMS): δ 8.67 (d, J = 4.4 Hz, 1H), 8.18 (d, J = 8.0 Hz, 1H), 7.82 (t, J = 7.8 Hz, 1H), 7.40 (t, J = 6.0 Hz, 1H), 7.09–7.07 (m, 4H), 6.90–6.82 (m, 4H), 6.18 (d, J = 7.6 Hz, 4H), 6.71 (m, 4H), 6.60–6.57 (m, 2H), 4.89 (s, 2H), 3.56–3.50 (m, 2H), 3.43–3.36 (m, 2H), 2.82–2.74 (m, 2H), 2.68–2.62 (m, 2H), 2.12 (s, 3H), 1.12 (s, 3H). ^{13}C NMR (101 MHz, $CDCl_3$) δ 145.36 (m), 144.27 (s), 141.88 (d, J = 9.5 Hz), 140.67 (s), 140.04 (s), 139.80 (d, J = 3.0 Hz), 139.39 (s), 138.71 (s), 138.42 (s), 137.13 (s), 135.83 (s), 134.49 (s), 131.46 (s), 131.11 (d, J = 11.2 Hz), 130.75 (s), 130.41 (d, J = 17.4 Hz), 129.91 (s), 129.63 (d, J = 7.4 Hz), 129.27 (s), 128.87 (s), 128.22 (s), 127.86 (s), 127.69–127.17 (m), 126.92 (d, J = 16.9 Hz), 126.52 (s), 126.19 (d, J = 9.5 Hz), 125.72 (s), 125.44 (s), 124.60 (s), 122.43 (s), 120.22 (s), 82.36 (s), 77.37 (s), 77.05 (s), 76.74 (s), 71.15 (s), 56.00 (s), 35.93 (s), 34.28 (s), 32.33 (s), 31.45 (s), 21.39 (s). Anal. calcd for $C_{44}H_{38}N_2(H_2O)$: C, 86.24; H, 6.58; N, 4.57%, found: C, 86.32; H, 6.32; N, 4.34%.

L2^{iPr}. Using same method as employed in the synthesis of **L1^{Me}**, a light-yellow product was collected (0.8 g, yield 39%). FT-IR (KBr, cm^{-1}): 3456 (w), 2956 (w), 2926 (w), 2878 (s), 1641 (ν(C=N), m), 1563 (ν(C=N), m), 1490 (m), 1445 (m), 1362 (m), 1298 (m), 1216 (m), 1161 (w), 1124 (s), 1099 (m), 1097 (m), 1009 (s), 883 (m), 719 (m), 842 (s), 946 (w), 761 (s), 685 (w). ^{1}H NMR (400 MHz, $CDCl_3$, TMS) δ 8.75 (s, 1H), 8.27 (s, 1H), 7.91 (s, 1H), 7.49 (s, 1H), 7.08 (d, J = 3.8 Hz, 4H), 6.99 (s, 4H), 6.92 (t, J = 8.4 Hz, 4H), 6.82 (s, 4H), 6.56 (s, 2H), 5.29 (s, 2H), 3.51 (t, J = 7.3 Hz, 2H), 3.36 (dd, J = 10.6, 5.8 Hz, 2H), 2.81 (s, 2H), 2.65 (d, J = 6.5 Hz, 2H), 1.27 (s, 1H), 1.10 (d, J = 5.7 Hz, 3H), 1.01 (d, J = 6.8 Hz, 6H). ^{13}C NMR (101 MHz, $CDCl_3$) δ 150.17–149.12 (m), 141.50–140.64 (m), 140.31–139.80 (m), 131.62 (s), 130.70 (s), 129.86 (s), 127.29 (s), 126.35 (d, J = 104.0 Hz), 77.38 (s), 76.95 (d, J = 23.0 Hz), 76.75 (s), 56.13 (s), 33.35 (s), 32.29 (s), 31.16 (s), 23.91 (s). Anal. calcd for $C_{46}H_{42}N_2(H_2O{\cdot}MeCOOEt)$: C, 82.38; H, 7.19; N, 3.84%, found: C, 82.14; H, 6.55; N, 3.67%.

L3^{tBu}. Using same method as employed in the synthesis of **L1^{Me}**, a light-yellow product was collected (0.2 g, yield 10%). FT-IR (KBr, cm^{-1}): 3648 (w), 3054 (w), 3016 (w), 2947 (m), 2893 (w), 1921 (w), 1647 (ν(C=N), s), 1566 (ν(C=N), m), 1491 (m), 1466 (w), 1457 (m), 1360 (s), 1304 (m), 1281 (m), 1101 (m), 955 (w), 844 (w), 782 (w), 770 (m), 749 (s), 717 (w). ^{1}H NMR (400 MHz, $CDCl_3$, TMS), 7.67 (d, J = 6.4 Hz, 1H), δ 7.91 (d, J = 8.1 Hz, 2H), 7.48 (d, J = 5.9 Hz, 2H), 7.31 (d, J = 5.4 Hz, 1H), 7.26 (s, 1H), 7.18 (s, 3H), 7.14 (d, J = 8.1 Hz, 2H), 7.08–7.04 (m, 6H), 6.54 (d, J = 7.3 Hz, 2H), 6.10 (d, J = 7.0 Hz, 2H), 5.37 (s, 2H), 3.46 (dd, J = 12.6, 6.6 Hz, 2H), 2.90 (d, J = 4.8 Hz, 1H), 2.49 (d, J = 3.8 Hz, 1H), 2.19 (dd, J = 13.9, 6.2 Hz, 2H), 1.89 (dd, J = 14.2, 7.7 Hz, 2H), 1.41–1.28 (m, 3H), 1.11 (s, 9H). ^{13}C NMR (151 MHz, $CDCl_3$) δ 149.24–147.43 (m), 141.03 (s), 139.62 (d, J = 58.7 Hz), 138.45–136.29 (m), 131.64 (s), 130.49 (s), 129.82 (s), 129.05 (s), 128.24 (s), 126.70 (d, J = 4.2 Hz), 126.16 (s), 125.75 (d, J = 13.9 Hz), 77.24 (s), 77.02 (s), 76.81 (s), 56.39 (s), 32.21 (s), 31.32 (s), 31.16 (s), 16.31 (s). Anal. calcd for $C_{47}H_{44}N_2$: C, 88.64; H, 6.96; N, 4.40%, found: C, 89.21; H, 6.38; N, 4.97%.

L4^{Bs}. Using the same method as employed in the synthesis of **L1^{Me}**, a light-yellow product was collected (0.5 g, yield 20%). FT-IR (KBr, cm^{-1}): 3013 (w), 2923 (m), 1643 (ν(C=N), s), 1565 (ν(C=N), m), 1490 (s), 1437 (m), 1361 (m), 1300 (m), 1258 (m), 1161 (w), 1100 (s), 1020 (m), 941 (w), 909 (w), 802 (m), 748 (s), 678 (w). ^{1}H NMR (400 MHz, $CDCl_3$, TMS) δ 8.67 (d, J = 4.8 Hz, 1H), 8.25 (d, J = 8.1 Hz, 1H), 7.41 (d, J = 6.9 Hz, 1H), 7.84 (t, J = 7.9 Hz, 1H), 7.15 (d, J = 7.3 Hz, 2H), 7.10–6.97 (m, 8H), 6.92 (t, J = 7.5 Hz, 2H), 6.82 (d, J = 8.2 Hz, 8H), 6.71 (d, J = 7.6 Hz, 2H), 6.54 (t, J = 7.7 Hz, 2H), 6.45 (s, 2H), 4.99 (s, 1H), 4.80 (s, 2H), 2.93 (d, J = 13.0 Hz, 2H), 2.77 (dd, J = 16.1, 8.9 Hz, 2H), 2.69–2.53 (m, 4H), 2.51–2.25 (m, 4H), 1.43 (s, 3H). ^{13}C NMR (101 MHz, $CDCl_3$) δ 161.30–160.37 (m), 140.13–139.45 (m), 139.45–139.13 (m), 139.03–138.37 (m), 130.11 (d, J = 19.5 Hz), 129.52 (s), 128.73 (s),

126.52–125.37 (m), 124.80 (d, J = 27.9 Hz), 76.31 (s), 76.00 (s), 75.68 (s), 31.28 (s). Anal. calcd for $C_{58}H_{48}N_2$ (MeCOOEt·H_2O): C, 84.27; H, 6.84; N, 3.28%, found: C, 84.42; H, 6.48; N, 3.26%.

Synthesis and characterization of nickel bromide complexes

Ni1^{Me}. A solution of ligand **L1^{Me}** (200 mg, 0.33 mmol) in DCM (10 mL) and EtOH (3 mL) was prepared, to which (DME) $NiBr_2$ (103 mg, 0.33 mmol) was added. The reaction mixture was stirred for approximately 12 h and then concentrated under reduced pressure. Excess diethyl ether was added to induce precipitation. The resulting dark-brown solid was washed with diethyl ether (3 × 5 mL) and filtered. Drying under reduced pressure for at least 24 h afforded **Ni1^{Me}** as a dark-brown solid (210 mg, yield 76%). FTIR (cm^{-1}): 3010 (w), 2915 (w), 2870 (w), 1617 (ν(C=N), m), 1592 (s), 1570 (w), 1491 (s), 1440 (s), 1373 (s), 1322 (s), 1257 (s), 1155 (m), 1097 (s), 1044 (w), 1027 (s), 874 (m), 831 (s), 740 (w), 721 (m), 688 (w). Anal. calcd for $C_{44}H_{38}N_2$-$NiBr_2$·H_2O: C, 63.57; H, 4.85; N, 3.37. Found: C, 63.55; H, 4.87; N, 2.98%.

Ni2^{iPr}. Using the same procedure for the synthesis of **Ni1^{Me}**, **Ni2^{iPr}** was collected as a dark-yellow powder (230 mg, yield 85%). FTIR (cm^{-1}): 3064 (w), 3014 (w), 2925 (w), 1621 (ν(C=N), m), 1595 (s), 1571 (w), 1489 (s), 1444 (s), 1369 (s), 1315 (s), 1257 (s), 1160 (s), 1121 (w), 1029 (s), 876 (m), 817 (m), 763 (m), 717 (m), 681 (w). Anal. calcd for $C_{46}H_{42}N_2NiBr_2$ MeOH: C, 64.63; H, 5.31; N, 3.21. Found: C, 64.13; H, 5.06; N, 3.17%.

Ni3^{tBu}. Using the same procedure for the synthesis of **Ni1^{Me}**, **Ni3^{tBu}** was collected as a dark-yellow powder (120 mg, yield 89%). FTIR (cm^{-1}): 3055 (w), 2953 (m), 2883 (m), 1622 (ν(C=N), m), 1596 (s), 1489 (s), 1444 (s), 1370 (s), 1315 (s), 1257 (s), 1218 (m), 1160 (s), 1099 (s), 1050 (m), 1026 (m), 878 (m), 852 (m), 822 (m), 718 (m). Anal. calcd for $C_{47}H_{44}N_2NiBr_2$ EtOH: C, 65.29; H, 5.59; N, 3.11. Found: C, 65.15; H, 5.90; N, 2.82%.

Ni4^{Bs}. Using the same procedure for the synthesis of **Ni1^{Me}**, **Ni4^{Bs}** was collected as a dark-brown powder (78 mg, yield 81%). FTIR (cm^{-1}): 3058 (w), 2928 (m), 1619 (ν(C=N), m), 1594 (s), 1491 (s), 1437 (s), 1368 (s), 1314 (s), 1255 (s), 1161 (m), 1100 (m), 1025 (m), 978 (w), 943 (w), 878 (w), 836 (m), 778 (s). Anal. calcd for $C_{58}H_{48}N_2NiBr_2$ DCM: C, 65.83; N, 2.60; H, 4.68. Found: C, 65.82; N, 2.71%; H, 4.74.

Ethylene polymerization procedure

Ethylene polymerization for entry 7 (Table 2) was carried out as follows: in a dried 250 mL reactor, **Ni1^{Me}** (1.627 mg, 2.00 μmol) was dissolved in toluene (25.0 mL). It was rinsed with 25 mL toluene to transfer all the precatalyst, followed by addition of another 25 mL to the reactor. DEAC (Al/Ni = 800) was added, followed by the addition of 25 mL of toluene, and the reactor was heated to 40 °C, charged with ethylene (10 atm), and stirred for 30 min at constant pressure. The mixture was quenched by adding a 10% (v/v) solution of hydrochloric acid in ethanol, washed with an excess amount of ethanol, filtered, dried at 60 °C under vacuum, and weighed. All other polymerizations were performed following the same procedure, with adjustments to the reaction conditions, as noted in the respective tables.

Conflicts of interest

There are no conflicts to declare.

Data availability

CCDC 2466367 (**Ni1^{Me}**) and 2466366 (**Ni2^{iPr}**) contain the supplementary crystallographic data for this paper.[38a,b]

Supplementary Information: The data supporting this article have been included as part of the SI. See DOI: **https://doi.org/10.1039/d5ra05407a**.

Acknowledgements

We acknowledge the support from the Strategic Priority Research Program of the Chinese Academy of Sciences, grant no. XDC0270101. We also acknowledge the support from the Chemistry and Chemical Engineering Guangdong Laboratory (2111018 and 2132012).

Notes and references

1 (*a*) L. K. Johnson, C. M. Killian and M. Brookhart, *J. Am. Chem. Soc.*, 1995, **117**, 6414–6415; (*b*) C. M. Killian, D. J. Tempel, L. K. Johnson and M. Brookhart, *J. Am. Chem. Soc.*, 1996, **118**, 11664–11665.

2 Z. Wang, Q. Liu, G. A. Solan and W.-H. Sun, *Coord. Chem. Rev.*, 2017, **350**, 68–83.

3 (*a*) S. A. Svejda, L. K. Johnson and M. Brookhart, *J. Am. Chem. Soc.*, 1999, **121**, 10634–10635; (*b*) M. D. Leatherman, S. A. Svejda, L. K. Johnson and M. Brookhart, *J. Am. Chem. Soc.*, 2003, **125**, 3068–3082.

4 (*a*) G. Zanchin and G. Leone, *Prog. Polym. Sci.*, 2021, **113**, 101342; (*b*) A. M. Doerr, M. R. Curry, R. C. Chapleski, J. M. Burroughs, E. K. Lander, S. Roy and B. K. Long, *ACS Catal.*, 2022, **12**, 73–81.

5 (*a*) A. Dashti and M. Ahmadi, *Macromol. Rapid Commun.*, 2024, **45**, 2300746; (*b*) F. S. Golub, V. A. Bolotov and V. N. Parmon, *Catal. Ind.*, 2021, **13**, 203–215.

6 R. M. Patel, P. Jain, B. Story and S. Chum, in *Innovations in Industrial and Engineering Chemistry*, 2008, ch. 4, pp. 71–102.

7 (*a*) Q. Mahmood, Z. Hu, G. Ren and W.-H. Sun, *Coord. Chem. Rev.*, 2025, **541**, 216833; (*b*) Q. Mahmood and W.-H. Sun, *R. Soc. Open Sci.*, 2018, **5**, 180367.

8 (*a*) L. Guo, S. Dai, X. Sui and C. Chen, *ACS Catal.*, 2016, **6**, 428–441; (*b*) Q. Muhammad, M. S. Bashir, S. Iqbal and Q. Mahmood, *Eur. Polym. J.*, 2021, **160**, 110783.

9 H. Mu, L. Pan, D. Song and Y. Lu, *Chem. Rev.*, 2015, **115**, 12091–12137.

10 Q. Mahmood, X. Li, L. Qin, L. Wang and W.-H. Sun, *Dalton Trans.*, 2022, **51**, 14375–14407.

11 (*a*) T. V. Laine, K. Lappalainen, J. Liimatta, E. Aitola, B. Löfgren and M. Leskelä, *Macromol. Rapid Commun.*, 1999, **20**, 487–490; (*b*) T. V. Laine, M. Klinga and M. Leskelä, *Eur. J. Inorg. Chem.*, 1999, **1999**, 959–965.

12 (*a*) L. Zhang, X. Hao, W.-H. Sun and C. Redshaw, *ACS Catal.*, 2011, **1**, 1213–1220; (*b*) Z. Chen, K. E. Allen, P. S. White,

O. Daugulis and M. Brookhart, *Organometallics*, 2016, **35**, 1756–1763; (*c*) E. Yue, L. Zhang, Q. Xing, X. P. Cao, X. Hao, C. Redshaw and W.-H. Sun, *Dalton Trans.*, 2014, **43**, 423–429; (*d*) E. Yue, Q. Xing, L. Zhang, Q. Shi, X. P. Cao, L. Wang, C. Redshaw and W.-H. Sun, *Dalton Trans.*, 2014, **43**, 3339–3347; (*e*) H. Fan, G. Xu, H. Wang and S. Dai, *J. Polym. Sci.*, 2022, **60**, 1944–1953; (*f*) H. Saeed, Q. Mahmood, Y. Ma, K. F. Tahir, G. Ren, Y. Wang and W.-H. Sun, *ChemCatChem*, 2025, e202401640.

13 W.-H. Sun, S. Song, B. Li, C. Redshaw, X. Hao, Y. S. Li and F. Wang, *Dalton Trans.*, 2012, **41**, 11999–12006.

14 C. Wang, Y. Zhang, H. Mu and Z. Jian, *Dalton Trans.*, 2020, **49**, 4824–4832.

15 M. Zada, A. Vignesh, L. Guo, R. Zhang, W. Zhang, Y. Ma, Y. Sun and W.-H. Sun, *ACS Omega*, 2020, **5**, 10610–10618.

16 A. Antonov, N. V. Semikolenova, E. P. Talsi, M. A. Matsko, V. A. Zakharov and K. P. Bryliakov, *J. Organomet. Chem.*, 2016, **822**, 241–248.

17 (*a*) J. Yu, Y. Zeng, W. Huang, X. Hao and W.-H. Sun, *Dalton Trans.*, 2011, **40**, 8436–8442; (*b*) G. B. Galland and W.-H. Sun, *Dalton Trans.*, 2015, **44**, 14281–14289; (*c*) R. Zhang, Z. Wang, Z. Flisak, X. Hao, Q. Liu and W.-H. Sun, *J. Polym. Sci., Part A: Polym. Chem.*, 2017, **55**, 2601–2609.

18 (*a*) S. Dai, X. Sui and C. Chen, *Chem. Commun.*, 2016, **52**, 9113–9116; (*b*) J. Gan and S. Dai, *Polym. Chem.*, 2025, **16**, 3172–3178.

19 (*a*) H. Zheng and H. Gao, *Macromolecules*, 2024, **57**, 6899–6913; (*b*) K. T. Mahmudov, A. V. Gurbanov, F. I. Guseinov and M. F. C. Guedes da Silva, *Coord. Chem. Rev.*, 2019, **387**, 32–46.

20 (*a*) Z. Cheng, H. Gao, Z. Qiu, H. Zheng, D. Li, L. Jiang and H. Gao, *ACS Catal.*, 2024, **14**, 7956–7966; (*b*) L. Falivene, T. Wiedemann, I. Göttker-Schnetmann, L. Caporaso, L. Cavallo and S. Mecking, *J. Am. Chem. Soc.*, 2018, **140**, 1305–1312; (*c*) F. Lin, M. Voccia, L. Odenwald, I. Göttker-Schnetmann, L. Falivene, L. Caporaso and S. Mecking, *J. Am. Chem. Soc.*, 2023, **145**, 27950–27957; (*d*) C. S. Popeney, A. L. Rheingold and Z. Guan, *Organometallics*, 2009, **28**, 4452–4463; (*e*) T. Vaidya, K. Klimovica, A. M. LaPointe, I. Keresztes, E. B. Lobkovsky, O. Daugulis and G. W. Coates, *J. Am. Chem. Soc.*, 2014, **136**, 7213–7216.

21 Y. Sun, M. Chi, M. S. Bashir, Y. Wang and M. Qasim, *New J. Chem.*, 2021, **45**, 13280–13285.

22 (*a*) A. Zhou, R. Yuan, Q. Mahmood, S.-F. Yuan, Y. Wang, Z. Hu, S. Zou, T. Liang and W.-H. Sun, *Polym. Chem.*, 2024, **15**, 4029–4043; (*b*) A. Khalid, Z. Hu, Y. Ma, Q. Mahmood, G. Ren, A. Razzaq, Y. Wang, T. Liang and W.-H. Sun, *Eur. Polym. J.*, 2025, **223**, 113635; (*c*) X. Li, Z. Hu, Q. Mahmood, Y. Wang, S. Sohail, S. Zou, T. Liang and W.-H. Sun, *Dalton Trans.*, 2024, **53**, 18193–18206; (*d*) L. Wang, M. Liu, Q. Mahmood, S. Yuan, X. Li, L. Qin, S. Zou, T. Liang and W.-H. Sun, *Eur. Polym. J.*, 2023, **194**, 112112.

23 (*a*) Y. Zhang, C. Huang, X. Wang, Q. Mahmood, X. Hao, X. Hu, C. Y. Guo, G. A. Solan and W.-H. Sun, *Polym. Chem.*, 2017, **8**, 995; (*b*) J. Guo, W. Zhang, Q. Mahmood, R. Zhang, Y. Sun and W.-H. Sun, *J. Polym. Sci., Part A: Polym. Chem.*, 2018, **56**, 1269.

24 (*a*) Q. Mahmood, Y. Zeng, E. Yue, G. A. Solan, T. Liang and W.-H. Sun, *Polym. Chem.*, 2017, **8**, 6416; (*b*) Q. Mahmood, Y. Zeng, X. Wang, Y. Sun and W.-H. Sun, *Dalton Trans.*, 2017, **46**, 6934–6947.

25 C. G. de Souza, R. F. de Souza and K. Bernardo-Gusmão, *Appl. Catal., A*, 2007, **325**, 87–90.

26 H. Gao, H. Hu, F. Zhu and Q. Wu, *Chem. Commun.*, 2012, **48**, 3312–3314.

27 I. E. Soshnikov, N. V. Semikolenova, K. P. Bryliakov, A. A. Antonov and E. P. Talsi, *Organometallics*, 2022, **41**, 1015–1024.

28 I. E. Soshnikov, N. V. Semikolenova, K. P. Bryliakov, A. A. Antonov, W.-H. Sun and E. P. Talsi, *Organometallics*, 2020, **39**, 3034–3040.

29 (*a*) G. J. P. Britovsek, S. A. Cohen, V. C. Gibson and M. van Meurs, *J. Am. Chem. Soc.*, 2004, **126**, 10701–10712; (*b*) Y. Zhang, Y. Zhang, X. Hu, C. Wang and Z. Jian, *ACS Catal.*, 2022, **12**, 14304–14320.

30 (*a*) L. Zhong, G. Li, G. Liang, H. Gao and Q. Wu, *Macromolecules*, 2017, **50**, 2675–2682; (*b*) G. Ren, R. Yuan, Q. Mahmood, Y. Zeng, Y. Wang, Z. Hu, S. Zou, T. Liang and W.-H. Sun, *J. Mol. Struct.*, 2024, **1316**, 139037.

31 (*a*) F. S. Liu, H. B. Hu, Y. Xu, L. H. Guo, S. B. Zai, K. M. Song, H. Y. Gao, L. Zhang, F. M. Zhu and Q. Wu, *Macromolecules*, 2009, **42**, 7789; (*b*) H. Saeed, Q. Mahmood, R. Yuan, Y. Wang, S. Zou, K. F. Tahir, Y. Ma, T. Liang and W.-H. Sun, *Polym. Chem.*, 2024, **15**, 1437–1452.

32 X. Wang, L. Fan, Y. Ma, C. Y. Guo, G. A. Solan, Y. Sun and W.-H. Sun, *Polym. Chem.*, 2017, **8**, 2785–2795.

33 L. Guo, W. Sun, S. Li, G. Xu and S. Dai, *Polym. Chem.*, 2019, **10**, 4866–4871.

34 (*a*) J. L. Rhinehart, L. A. Brown and B. K. Long, *J. Am. Chem. Soc.*, 2013, **135**, 16316–16319; (*b*) L. A. Brown, W. C. Anderson, N. E. Mitchell, K. R. Gmernicki and B. K. Long, *Polymers*, 2018, **10**, 41.

35 (*a*) R. K. Wang, X. L. Sui, W. M. Pang and C. L. Chen, *ChemCatChem*, 2016, **8**, 434–440; (*b*) F. S. Liu, H. B. Hu, Y. Xu, L. H. Guo, S. B. Zai, K. M. Song, H. Y. Gao, L. Zhang, F. M. Zhu and Q. Wu, *Macromolecules*, 2009, **42**, 7789–7796.

36 (*a*) M. Qasim, C. Tan and C. Chen, *Sci. Bull.*, 2020, **65**, 300–307; (*b*) R. Yuan, Y. Wang, Q. Mahmood, Y. Zeng, L. Qin, S. Zou, T. Liang and W.-H. Sun, *Polymer*, 2024, **293**, 126690.

37 (*a*) Y. He, X. Qiu, J. Klosin, R. Cong, G. R. Roof and D. Redwine, *Macromolecules*, 2014, **47**, 3782; (*b*) V. Busico, R. Cipullo, N. Friederichs, H. Linssen, A. Segre, V. V. A. Castelli and G. V. D. van der Velden, *Macromolecules*, 2005, **38**, 6988.

38 (*a*) A. Khalid, Q. Mahmood, A. Razzaq, Y. Ma, G. Ren, Y. Wang, T. Liang and W.-H. Sun, CCDC 2466366: Experimental Crystal Structure Determination, 2025, DOI: **10.5517/ccdc.csd.cc2nsg64**; (*b*) A. Khalid, Q. Mahmood, A. Razzaq, Y. Ma, G. Ren, Y. Wang, T. Liang and W.-H. Sun, CCDC 2466367: Experimental Crystal Structure Determination, 2025, DOI: **10.5517/ccdc.csd.cc2nsg75**.